Understanding the Nature of the DNA-Assisted Separation of Single-Walled Carbon Nanotubes Using Fluorescence and Raman Spectroscopy

ARTICLE *in* NANO LETTERS · APRIL 2004

Impact Factor: 13.59 · DOI: 10.1021/nl034937k

7 AUTHORS, INCLUDING:

Ming Zheng
Fourth Military Medical University
78 PUBLICATIONS **5,247** CITATIONS
SEE PROFILE

Anand Jagota
Lehigh University
135 PUBLICATIONS **7,205** CITATIONS
SEE PROFILE

Daniel A Heller
Memorial Sloan-Kettering Cancer Center
69 PUBLICATIONS **3,774** CITATIONS
SEE PROFILE

Paul W Barone
Massachusetts Institute of Technology
52 PUBLICATIONS **4,844** CITATIONS
SEE PROFILE

NANO LETTERS

2004
Vol. 4, No. 4
543−550

Understanding the Nature of the DNA-Assisted Separation of Single-Walled Carbon Nanotubes Using Fluorescence and Raman Spectroscopy

Michael S. Strano,*,† Ming Zheng,‡ Anand Jagota,‡ G. Bibiana Onoa,‡ Daniel A. Heller,† Paul W. Barone,† and Monica L. Usrey†

Department of Chemical and Biomolecular Engineering, University of Illinois at Urbana-Champaign, Urbana, Illinois 61801, and DuPont Central Research and Development, Experimental Station, Wilmington, Delaware 19880

Received October 24, 2003; Revised Manuscript Received January 27, 2004

ABSTRACT

Certain DNA sequences form a highly stable monolayer at the surface of single-walled carbon nanotubes, enabling their dispersion in aqueous solution. Ion-exchange chromatography can be used to separate these systems on the basis of their diameter in distinct, eluted fractions. Raman and fluorescence spectroscopy are used to characterize the nature of the separation by a comparison of radial breathing mode intensities at 457-, 532-, 633-, and 785-nm excitation wavelengths. Trends reveal a strong diameter dependence of the fractions, with larger diameters eluting later than smaller diameters. Average diameters of each fraction varied from 0.816 and 1.084 nm for the first and last eluted fractions, respectively. This conclusion is supported by a systematic shifting of the Raman tangential mode with increasing elution as well as changes in the relative intensities of radial breathing modes. Fluorescence emission from each fraction reveals the absence of relative shifting or broadening and hence uniformity in the chemical environment and the absence of doping-related complications for each fraction. The separation also reveals the fine structure of the G′ two-phonon mode, which is described using a composite model with contributions from transition-dependent phonons.

1.0. Introduction. The most significant hurdle to the application of single-walled carbon nanotubes as novel electronic materials[1] is their separation according to their chiral vector.[2−7] All known preparative methods lead to polydisperse materials of semiconducting, semimetallic, and metallic electronic types. Recent advances in the solution-phase processing[8,9] and spectroscopic identification using fluorescence[10] and Raman spectroscopy[11] have greatly improved the ability to monitor distinct nanotubes while in suspended mixtures. Definitive assignments of the optical features of semiconducting[10] as well as metallic and semimetallic species[11] provide a means of characterizing separations in detail. The source of this diversity in the electronic structure of these systems is the quantinization of the electronic wave vector of the 1-D system through the conceptual rolling of a graphene plane into a cylinder forming the nanotube.[12−15] The vector in units of hexagonal elements connecting two points on this plane defines the nanotube chirality in terms of two integers: n and m. When $|n - m| = 3q$, where q is an integer, the nanotube is metallic or semimetallic, and the remaining species are semiconducting with a geometry-dependent band gap.

Recent work has demonstrated that DNA sequences rich in guanine and thymidine amino acids adsorb strongly to carbon nanotube surfaces with a remarkable ability to self-assemble into ordered, helical monolayers.[6,7] This greatly enhances the formation of stable aqueous dispersions. Ion-exchange chromatography has been used to adsorb the dispersed mixture on a charged resin with a salt gradient elution, leading to the fractionation of optical features known to be distinct for particular (n, m) nanotubes.[8,9] The carbon nanotube is believed to perturb the charge distribution of the DNA polyelectrolyte either geometrically by changing the wrapping diameter or electronically by providing some charge shielding depending upon the polarizability of the nanotube. A clearer understanding of these two influences can come about by examining the nature of the separation (i.e., the underlying basis for preferential elution). This is the focus of the present work.

Raman spectroscopy has been used extensively to characterize solid and solution-dispersed carbon nanotubes.[16−23] Radial breathing modes (RBM) are low-wavenumber phonons corresponding to the symmetric expansion and contraction

* Corresponding author. E-mail: strano@uiuc.edu.
† University of Illinois at Urbana-Champaign.
‡ DuPont Central Research and Development.

10.1021/nl034937k CCC: $27.50
Published on Web 03/12/2004

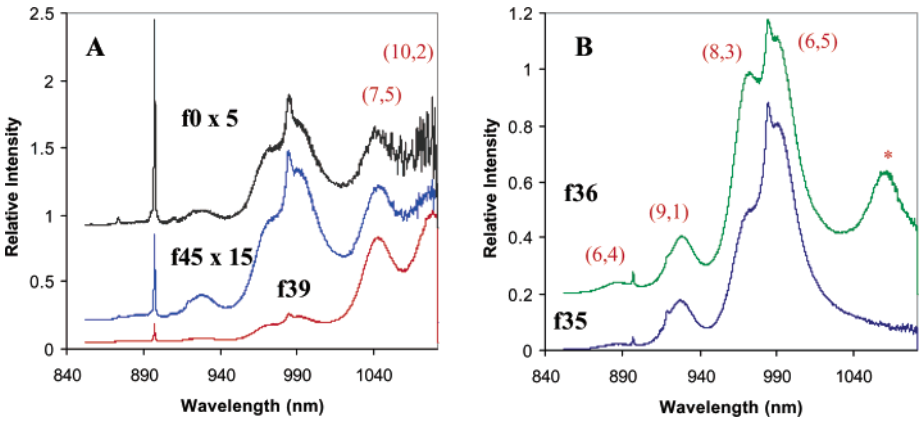

Figure 1. Partial fluorescence spectrum of eluted column fractions at 785 nm excitation: (A) starting material f0 and later fractions f45 and f39; (B) earlier fractions f35 and f36, including the assignment of fluorescence features.

of the nanotube in a radial manner. The Raman shift of these features is strongly diameter-dependent and can be used to track the separation of particular (*n*, *m*) nanotubes. Spectrofluorimetry can be used experimentally to resolve and characterize semiconducting components in a mixture with the direct measurement of the optical band gap.[8] This work seeks to use these spectroscopic tools to analyze fractions eluted from the ion-exchange column to determine the nature of the separation.

2.0. Experimental Section. Samples were dispersed using a 30-mer custom-synthesized DNA sequence of alternating guanine and thymidine amino acids under temperature-controlled ultrasonication conditions, as reported previously.[6] This solution was purified by centrifugation and injected into an HQ20 anion-exchange column (Applied Biosystems) where fractions were eluted using a salt gradient. The fractions are the same as those labeled in reference 6. Briefly, f0 represents the starting mixture, and f35, f36, f39, and f45 are four selected fractions eluted sequentially. These fractions were isolated, concentrated, and resuspended in equal volumes of D_2O for spectroscopic characterization.

Samples were characterized in solution by transferring them to a quartz cuvette. Raman spectroscopy was performed at 532- and 785-nm excitations using a Kaiser Optical RXN spectrometer at 10× magnification with 32 and 100 mW at the sample for each wavelength, respectively. Spectra generated at 633 and 514.5 nm were obtained using a setup from Renishaw fitted with a macroscopic sampling kit, a 50× (long) objective, and 15 mW of power at the sample. Excitation at 457, 496, and 502 nm was performed using a Lexel 95 water-cooled Ar^+ laser (20 mW at the sample) and a Spex triple-grating 1870 spectrometer with a liquid-N_2-cooled CCD array detector. Spectroscopic-grade cyclohexane (Sigma-Aldrich) was used in the same geometric configuration as an intensity calibration standard.[24] Each Raman spectrum in the region from 175 to 400 cm^{-1} was deconvoluted using a summation of Lorentzian peak shapes. Where it is indicated, spectra were normalized to the Raman scattering of the solvent, D_2O, for comparison.

3.0 Results and Discussion. *3.1. Analysis of Carbon Nanotube Fluorescence.* We track four samples that were eluted from the column sequentially: f35, f36, f39, and f45, with f0 representing the starting injected material. The absorption spectra of these fractions have been published previously.[6] Partial fluorescence spectra were generated at 785 nm excitation and were limited to 1100 nm by the detector range of the CCD. This range probes the smallest-diameter semiconducting species produced in the HiPco process.[25] Figure 1, parts A and B, shows the resulting spectra, which demonstrate the absence of a relative bathochromic shift with emission maxima coinciding for all fractions. As observed previously, the spectra are generally red-shifted in comparison to the spectrum of nanotubes in a sodium dodecyl sulfate environment.[8] The lack of relative shift indicates that the surface coverage and orientation of the DNA adsorbed phase is the same for each eluted fraction. We performed spectrophotometric titrations on each sample to ensure that surface protonation[26] is not playing a role in the apparent optical property difference. This rules out the possibility that aggregation[8] or electron localization[26] could account for the spectral differences between the fractions. The starting fraction is typical of previously published fluorescence spectra except for the noted red shift.[9] The shift in this case is likely due to incomplete surface coverage of the oligonucleotide strand at the surface of the nanotube, which allows water to permeate the absorbed layer and interact with the excited state of the SWNT. This model is consistent with proposed conformations of the absorbed phase for these DNA−SWNT hybrid systems[6] as well as AFM evidence showing gaps in the surface coverage. We have previously correlated this shift with the surface coverage of surfactants.[8]

The first two fractions f35 and f36[27] are notably strong in the (8, 3) and (9, 1) species, but f39 is correspondingly weak in these nanotubes. The last fraction f45 shows a general diminishment of all fluorescent species in the region probed by the CCD detector. The fact that all samples demonstrate photoluminescence is strong evidence that they have redispersed as individual nanotubes and that they can be characterized via the solution phase.[10,11] Raman spectroscopy can be interpreted as that from individually isolated nanotubes. Figure 1, parts A and B, shows spectroscopic assignments for the fluorescence features as published previously.[9]

3.2. Raman at Low Wavenumbers: Diameter Distributions from an Analysis of Radial Breathing Modes. Resonance Raman spectroscopy has great utility in that individual

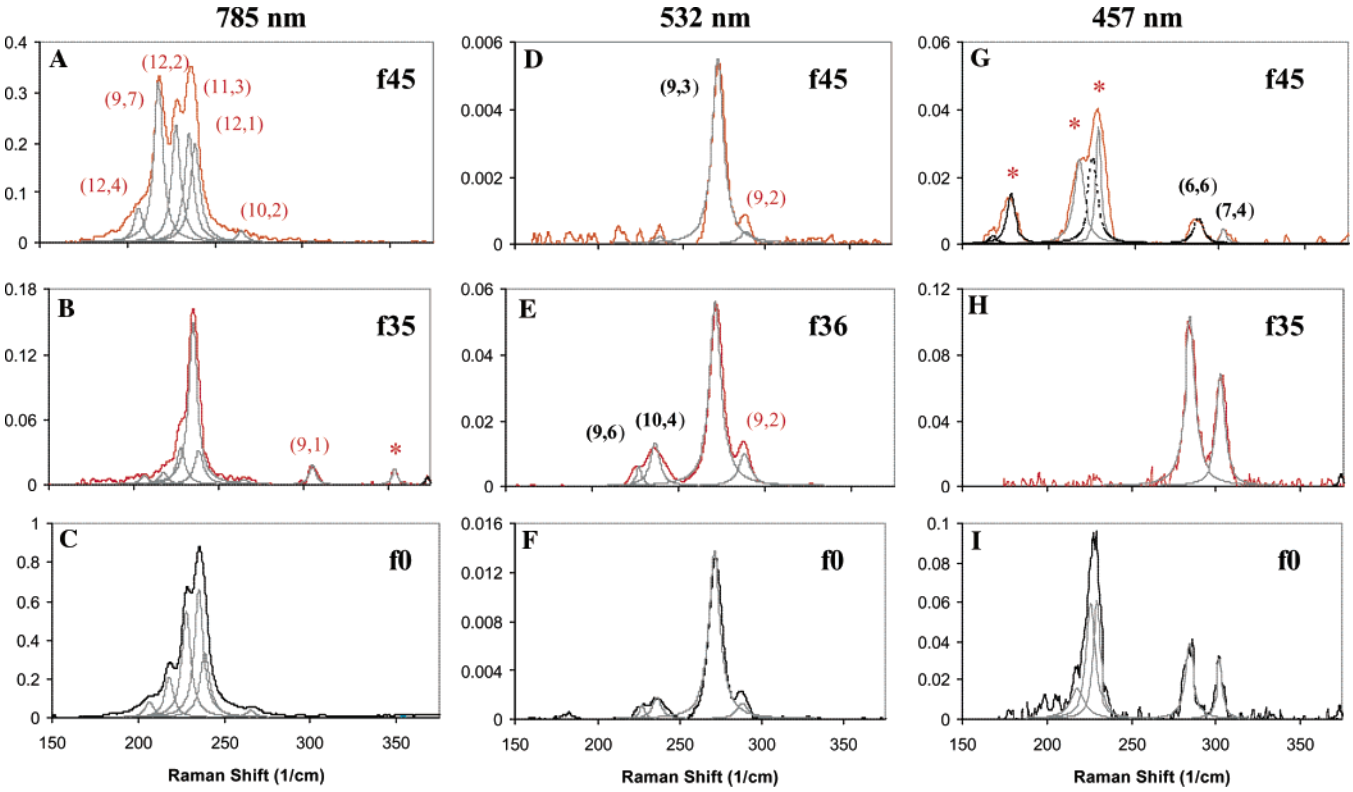

Figure 2. Low-wavenumber Raman spectra at 785, 532, and 457 nm excitation for the starting material f0 and the first f35/f36 and the last f45 eluted fractions.

metallic nanotube species can be probed relative to semiconductors, and this can shed some light on the nature of a possible electronic-based separation.[3,4,10,11] Figure 2 is a compilation of three different excitation wavelengths for the first and last eluted fractions compared to the starting material. At 785 nm, the excitation is resonant with the v2 → c2 transitions of exclusively semiconducting species. Compared to features of the starting fraction, we see that low-wavenumber features are enhanced in the latest fraction, and the opposite is true for the first fraction. The first fraction has intense features corresponding to the smallest-diameter species in the sample (i.e., (9, 1)). The marked unassigned peak is tentatively assigned (7, 2), with transitions at 821 and 627.8 nm and ω_{RBM} at 356 cm^{-1}. It is notable that these modes are barely detectable in the starting material but significantly enhanced in f35 and f36 (not shown). These observations are also consistent with Figure 1 in that smaller-diameter features are more prominent in earlier eluted fractions. At 532-nm excitation, radial breathing modes in the intermediate range, (9, 6) and (10, 4), are not prominent in later fractions but are in f36. (f35 shows a distribution similar to that of f0.) At this excitation, all but the longest-wavenumber feature (9, 2) are metallic. At 457 nm long-wavenumber features are metallic, and the shorter-wavenumber features correspond to the v3 → c3 resonance of semiconductors (indicated by *). We note that the latter are exceptionally strong in f45 but absent in f35 and not apparent in the starting material.

These radial breathing mode frequencies are strongly diameter-dependent according to the following relation determined empirically.[10,14,20,21]

$$\omega_{RBM} = \frac{C_1}{d_t} + C_2 \qquad \text{with } d_t = \frac{\sqrt{3}a_c\sqrt{n^2 + m^2 + mn}}{\pi}$$

Here, d_t is the nanotube diameter, a_c is the mean carbon−carbon bond length (0.144 nm in this work), and C_1 and C_2 are 223.5 (nm cm^{-1}) and 12.5 (cm^{-1}).[10,11] Hence, the trend in Figure 2 appears to be that later fractions contain an enrichment of larger-diameter species. This is supported by the 785-nm data and explains the behavior at 532-nm excitation if the intermediate modes are concentrated to the greatest extent in f36. At this excitation, there are no large-diameter species resonant with the laser to be enriched at f45. Hence, this last fraction simply shows a diminishment in RBM intensities. At 457 nm, larger-diameter (smaller-wavenumber) features are clearly more intense in later fractions, and these happen to correspond to higher transitions (v3 → c3) of semiconducting nanotubes.

3.3. Simultaneous Monitoring of Metals and Semiconductors. Because of the way in which electronic transitions scale with diameter, it is also possible at this point that later fractions are simply enriched in semiconducting nanotubes. To address this question, spectroscopy was performed at a transitional wavelength resonant with both metals and semiconductors.[10,11] At 633 nm in Figure 3a, the metals (bold) and semiconductors are labeled by the (n, m) index assigned previously.[10,11] Figure 3 shows the 633-nm low-wavenumber spectra for all fractions at this excitation. We note that diameter-based enrichment is also supported in these spectra,

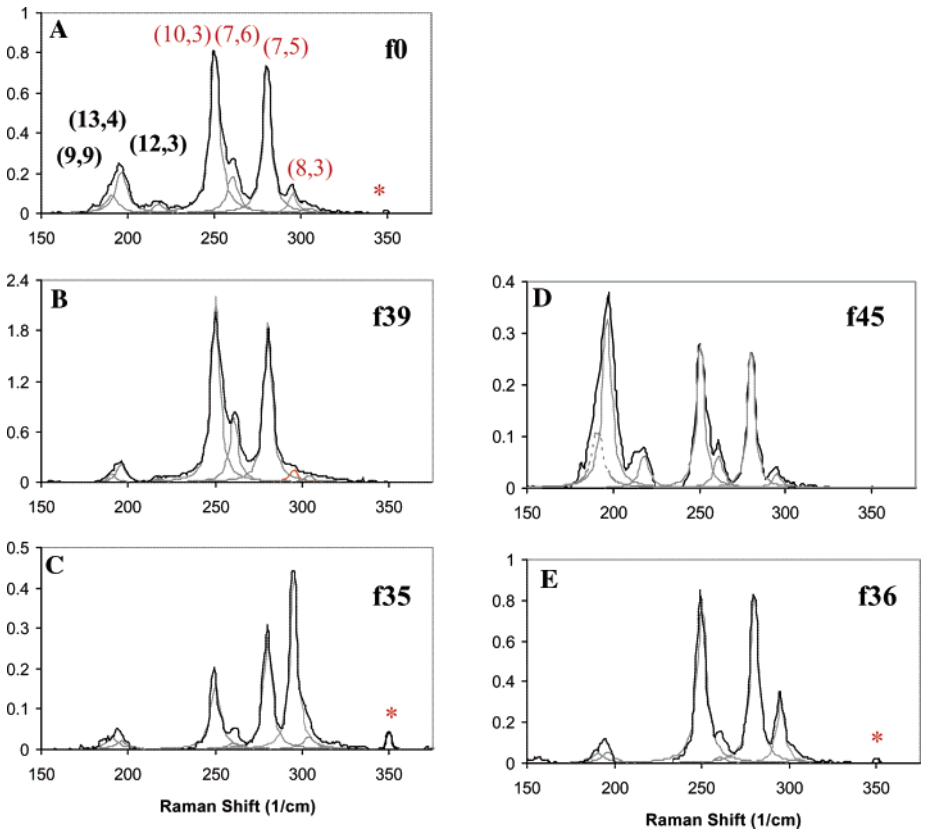

Figure 3. Low-wavenumber Raman spectra at 633 nm for all four fractions and the starting material.

with the larger-diameter species enriched in the last fraction whereas smaller-diameter species appear in f35 and f36. In this case, the electronic enrichment is the opposite of that in the 457-nm spectra: metallic nanotubes are enriched in later fractions in the 633-nm series. In the first fraction, f35, we again see the enrichment of one small species, which we tentatively assign as (7, 2) with a v2 → c2 transition at 627.8 nm (near the excitation wavelength.) It is not prominent in the starting material and therefore is enriched in these earlier fractions. Because at this wavelength the trends with respect to electronic structure are apparently reversed (metallic nanotubes are larger in diameter and semiconductors are smaller in diameter in this case), this behavior supports the previous observation that fractions are eluting primarily from smaller to larger diameter.

3.4. Tangential Mode. This diameter dependence is also reflected in an analysis of the tangential mode[28] at four different excitation wavelengths (Figure 4a−d.) This feature near 1590 cm^{-1} has been well studied[21−23] and is actually a composite with circumferential and axial components. The diameter dependence of the former is quite strong and follows an inverse relationship. In Figure 4A, the convolution of these features in successive fractions is seen as a general shifting from low wavenumbers to larger, corresponding to smaller- and then larger-diameter nanotubes with increasing elution fraction. It is noteworthy that the trend is in agreement with the above observation: as elution proceeds, the shift is to higher wavenumbers and hence larger-diameter species. The behavior is independent of the metallic or semiconducting nature of the nanotubes. For metallic nanotubes, the tangential mode splits into circumferential and axial components, where the former couples to the continuum of electronic states near the Fermi level, creating a Breit−Wigner−Fano line shape with a peak mode shifted to a lower Raman shift.[23] The extent of this shift depends on the availability of electrons near the Fermi level, but for undoped, deprotonated[26] nanotubes that are well dispersed (not aggregated), this peak mode reflects the diameter distribution in the sample. In Figure 4b, we also see that this frequency shifts with increasing elution. In Figure 4C at 514.5 nm, this dependence on the Fano line shape is also seen. At 633 nm (Figure 4D), we note that the Fano line shape is absent for the early fraction as the enrichment of small diameters decreases the population of metallic nanotubes resonant with this laser wavelength.

In these early fractions at 633-nm excitation, we also observe a feature near 1650 cm^{-1} that is enhanced. We tentatively assign these modes to high-wavenumber E_2 modes of chiral, small-diameter semiconductors on the basis of the work of Reich and co-workers.[29] In this work, we note that they are prominent in the early eluted fractions. This is supported by an analysis of spectra published earlier[16] that also show these features occurring in the absence of a Fano line shape for small bundles of larger-diameter nanotubes.

3.5. G′ Peak. The G′ peak originates from a dispersive, two-phonon process corresponding to a double-resonance condition.[21,22,30] In addition to the incident laser energy dependence, the Raman shift of this peak has a diameter

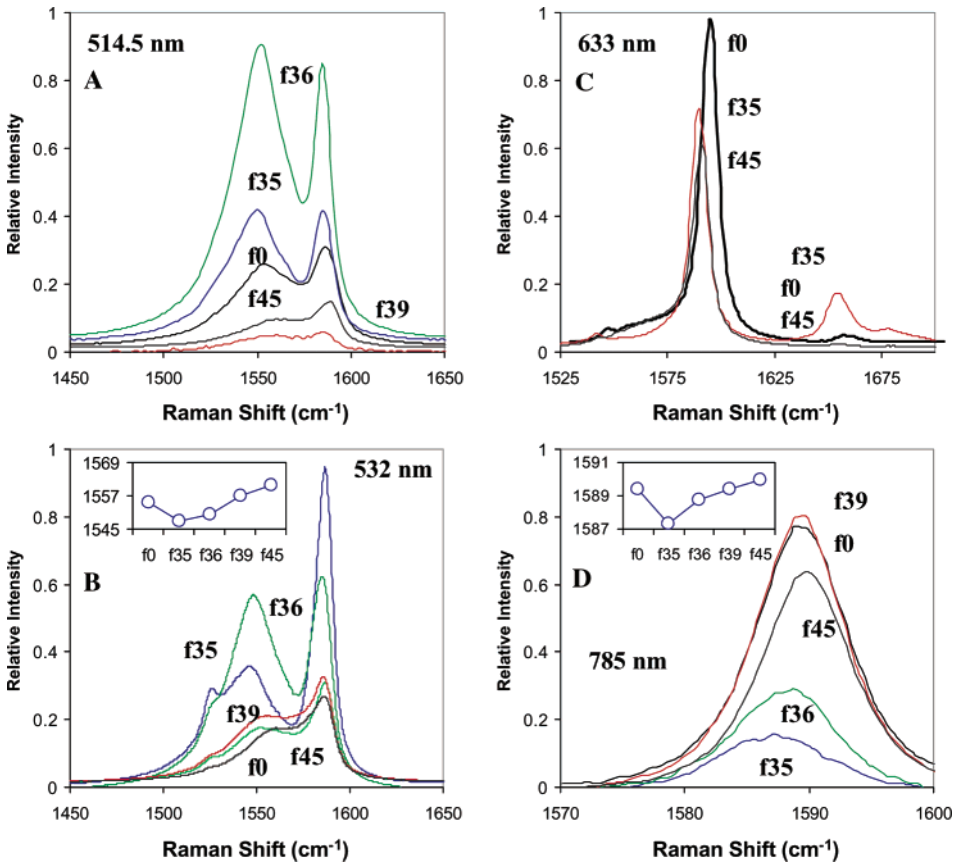

Figure 4. Tangential-mode region at four different excitation wavelengths: 514.5, 532, 633, and 785 nm for all fractions.

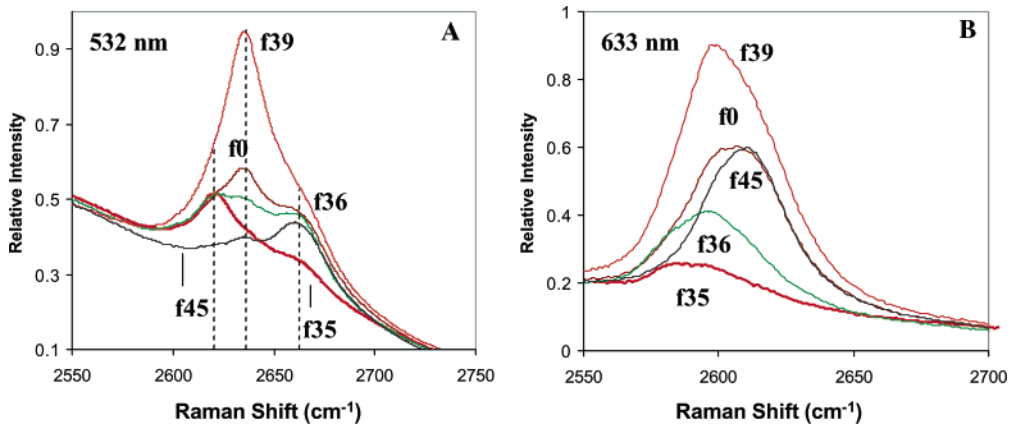

Figure 5. Two-phonon G′ mode region at 532- and 633-nm excitation. Spectra have been normalized with respect to D_2O. Raman peak near 2450 1/cm. This solvent accounts for the sloping baseline.

dependence of similar functional form to the G peak. The Raman shift depends on the laser energy, with a linear trend in excitation as reported previously.[19] We find in Figure 5 that the G′ behavior, also diameter-dependent, shows an increasing shift with increasing elution. At 633 nm, the number of nanotubes resonant with the laser is large, and this convolutes the various contributions to this feature. Conversely, at 532 nm (Figure 5B) a smaller distribution is found. Here we see significant fine structure of the G′ mode with three components labeled at 2622, 2636, and 2662 cm^{-1}. The essential bifurcation of this feature for single nanotubes has been described using a double-resonance model where the incident phonon is resonant with an interband transition and $|E_{laser} - E_{phonon}|$ is also resonant.[18,31] In this work, the scattered phonons have energies near 2 eV, which would be in resonance with either the (11, 1) or (10, 3) nanotubes in the sample. However, the eluted fractions still represent ensembles of species, and the G′ contributions due primarily to incident photons should dominate. Nanotubes in this sample have diameters that are too small to possess electronic transitions spaced by the phonon energy of one nanotube.[25,32] Instead, we claim that this structure is inhomogeneous in nature and reflects the different diameter populations in the sample. Particularly, it has been noted previously that the

peak position of this feature scales with inverse diameter and with different proportionality constants for distinct interband transitions. In this sample, this yields the three distinct populations evident for this feature. The (10, 4) and (9, 6) nanotubes are similar in diameter at 0.991 and 1.038 nm, respectively. Both are resonant at 532 nm via v1 → c1 (metal) transitions and are therefore assigned to the 2636-cm^{-1} feature. The smaller (9, 3) with a diameter of 0.858 nm may constitute a distinct contribution and would be 2662 cm^{-1}. Semiconductor (9, 2) or (10, 0) at 0.805 nm is resonant with its v2 → c2 transition and should therefore scale differently as the remaining 2622-cm^{-1} contribution.[33]

We note that in normalizing these fractions to their solvent D−O Raman mode, f39 is considerably more concentrated than the starting material. This may be an artifact of the reconcentration process that attempted to equalize the total added volume but apparently created disparities in the concentrations of SWNT material.[6,7] Nontube impurities, particularly fullerene fragments, may elute from the column first and change the mass concentration of the early fractions. All of the above analysis in this work considers relative peak intensities or shifts and is therefore unaffected by this disparity with this one fraction.

3.6. Intensity Comparison of Raman-Active Modes. This lack of solvatochromic shifting of fractions relative to each other also means that Raman intensities in each fraction can be compared directly because transitions for each (*n*, *m*) nanotube do not appear to be perturbed relative to the starting material. A simplified resonance condition for the RBM Raman-active mode is given by

$$I(E_{\text{laser}}) = \frac{Mc_{\text{o}}}{\left((E_{\text{laser}} - E_{ii})^2 - \frac{\Gamma^2}{4}\right)\left((E_{\text{laser}} - E_{\text{phonon}} - E_{ii})^2 - \frac{\Gamma^2}{4}\right)}$$

assuming that the density of states can be approximated as a summation of singularities at the transition energies E_{ii}. Here E_{laser}, E_{phonon}, and E_{ii} are the laser, phonon, and optical transition energies, respectively. The Γ parameter reflects the measurable peak broadening and prevents mathematical singularities in the above expression.[34] The parameter M is a factor including the total cross section with the assumption that $dM/dE_{\text{laser}} = 0$. The fluorescence results indicate that the broadening of the resonance window, Γ, is constant with each elution fraction, as evidenced by comparable line widths in the absorption spectrum. The transition energies coincide for each fraction because there is no peak shifting (E_{ii} is constant.) Hence, an (*n*, *m*) nanotube feature *i* of intensity $I(E_{\text{laser}})$ in fraction f*n* can be normalized against its intensity in the starting material, f0, yielding

$$EF_i = \frac{I(E_{\text{laser}})_{fn}}{I(E_{\text{laser}})_{f0}} = \left(\frac{c_{fn}}{c_{f0}}\right)_i$$

This comparison then gives a relative measure of sample enrichment in each fraction. We define this ratio as an enrichment factor supported by the following observations: the transition energies are apparently unperturbed from fraction to fraction, equal volumes were used for resuspension after column elution, and the four eluted fractions have average properties whose sum yields the relative peak intensities of the starting material. Figure 6 plots the enrichment factor for three small-diameter, metallic nanotubes, indicating that this parameter can be reliably measured within error to describe the separation qualitatively.

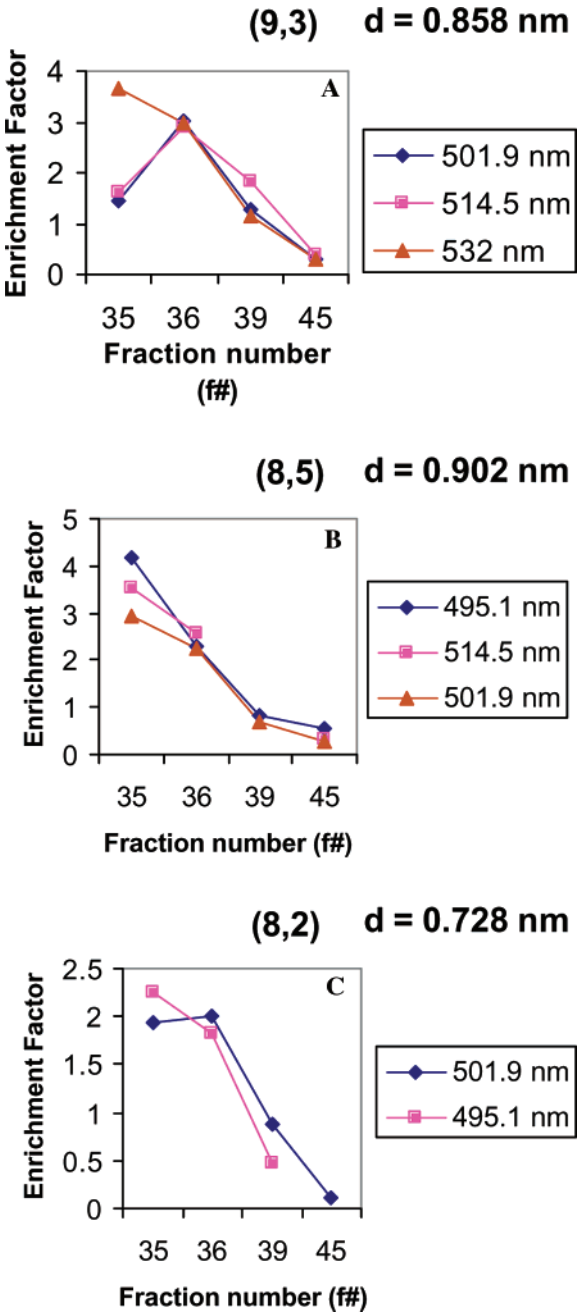

Figure 6. Enrichment factors probed with different excitation energies for three metallic carbon nanotubes: (9, 3), (8, 5), and (8, 2). Except for 532-nm excitaiton in fraction f35 for (9, 3), the enrichment index provides a reliable measure of separation.

To quantify the change in diameter with each fraction, we define an enrichment-factor-weighted mean diameter as

a normalized weighted sum over all N nanotubes probed at different Raman wavelengths:

$$\bar{d} = \frac{\sum_{i=1}^{N}\left(\frac{c_{fn}}{c_{f0}}\right)_i C_T f(d_i)\, d_i}{\sum_{i=1}^{N}\left(\frac{c_{fn}}{c_{f0}}\right)_i C_T f(d_i)} = \frac{\sum_{i=1}^{N} EF_i f(d_i)\, d_i}{\sum_{i=1}^{N} EF_i f(d_i)}$$

where

$$f(d_i) = \frac{1}{\sigma\sqrt{4\pi}} \exp\left(-\frac{(d_i - d_m)^2}{4\sigma^2}\right)$$

Here we model the distribution in starting concentration as a normal distribution with the mean diameter, d_m, centered at 0.93 nm and a standard deviation of $\sigma = 0.2$.[20] From the data set provided in this work, $N = 27$. The parameter C_T is the total nanotube concentration in the sample and is arbitrary in this case.

The unweighted mean diameter of this entire population is calculated to be 0.93 nm. We note that this is close to the mode in diameter distribution reported on the basis of spectrofluorimetry[10] and gives us confidence that the sampling of excitation wavelengths yields an appropriate representation of sample diameters. From these enrichment factors, we calculate average diameters of 0.816 nm for f35, 0.884 nm for f36, 0.958 nm for f39, and 1.084 nm for f45. This systematic change in mean diameter with increasing elution is consistent with the spectroscopic evidence reported above.

4.0. Conclusions. We have characterized single-walled carbon nanotubes separated by a process of DNA assembly and subsequent fractionation via preferential elution from an ion-exchange column. Fluorescence emission is detected from all eluted samples after resuspension, indicating that the material disperses primarily as individual nanotubes for all fractions. We observed no relative bathochromic shift, indicating that all fractions were in essentially the same chemical environment. This allows us to compare the Raman scattering intensities relative to those of the starting material because the resonant excitation window for each tube was the same in each fraction. An analysis of the radial breathing modes at different excitations reveals a strong diameter dependence in the fractionation. Smaller diameters eluted from the column first, and larger diameters were concentrated in the last fractions. This observation is supported by an examination of tangential mode and G′ phonon mode shifting because these features are known to be composites from an ensemble of diameters. The spectral evidence supports a separation based on linear surface charge density, which was modeled in earlier work as depending on the diameter of a helically wound charged polymer, essentially independent of length.

Acknowledgment. We acknowledge partial funding for this work from the DuPont CR&D Molecular Electronics Group and from the NSF (grant number CTS-0330350).

References

(1) Avouris, P. *Acc. Chem. Res.* **2002**, *35*, 1026−1034.
(2) Strano, M. S.; Dyke, C. A.; Usrey, M. L.; Barone, P. W.; Allen, M.; Shan, H.; Kittrel, C.; Hauge, R. H.; Tour, J. M.; Smalley, R. E. *Science* **2003**, *301*, 1519−1522.
(3) Krupke, R.; Hennrich, F.; von Lohneysen, H.; Kappes, M. M. *Science* **2003**, *301*, 344−347.
(4) Chattopadhyay, D.; Galeska, L.; Papadimitrakopoulos, F. A *J. Am. Chem. Soc.* **2003**, *125*, 3370−3375.
(5) Chen, Z.; Du, X.; Du, M. H.; Rancken, C. D.; Cheng, H. P.; Rinzler, A. G. *Nano Lett.* **2003**, *3*, 1245−1249.
(6) Zheng, M.; Jagota, A.; Strano, M. S.; Santos, A. P.; Barone, P.; Chou, S. G.; Diner, B. A.; Dresselhaus, M. S.; McLean, P. S.; Onoa, G. B.; Samsonidze, G. G.; Semke, E. D.; Usrey, M. L.; Walls, D. J. *Science* **2003**, *302*, 1545−48.
(7) Zheng, M.; Jagota, A.; Semke, E. D.; Diner, B. A.; McClean, R. S.; Lustig, S. R.; Richardson, R. E.; Tassi, N. G. *Nat. Mater.* **2003**, *2*, 338−342.
(8) Strano, M. S.; Moore, V. C.; Miller, M. K.; Allen, M. J.; Haroz, E. H.; Kittrel, C.; Hauge, R. H.; Smalley, R. E. *J. Nanosci. Nanotechnol.* **2003**, *3*, 81−86.
(9) O'Connell, M. J.; Bachilo, S. M.; Huffman, C. B.; Moore, V. C.; Strano, M. S.; Haroz, E. H.; Rialon, K. L.; Boul, P. J.; Noon, W. H.; Kittrell, C.; Ma, J. P.; Hauge, R. H.; Weisman, R. B.; Smalley, R. E. *Science* **2002**, *297*, 593−596.
(10) Bachilo, S. M.; Strano, M. S.; Kittrell, C.; Hauge, R. H.; Smalley, R. E.; Weisman, R. B. *Science* **2002**.
(11) Strano, M. S.; Doorn, S. K.; Haroz, E. H.; Kittrell, C.; Hauge, R. H.; Smalley, R. E. *Nano Lett.* **2003**, *3*, 1091−1096.
(12) Mintmire, J. W.; White, C. T. *Phys. Rev. Lett.* **1998**, *81*, 2506−2509.
(13) Reich, S.; Thomsen, C. *Phys. Rev. B* **2000**, *62*, 4273−4276.
(14) Saito, R.; Dresselhaus, G.; Dresselhaus, M. S. *Physical Properties of Carbon Nanotubes*; Imperial College Press: London, 1998.
(15) Saito, R.; Dresselhaus, G.; Dresselhaus, M. S. *Phys. Rev. B* **2000**, *61*, 2981−2990.
(16) Yu, Z. H.; Brus, L. E. *J. Phys. Chem. B* **2001**, *105*, 6831−6837.
(17) Sauvajol, J. L.; Anglaret, E.; Rols, S.; Alvarez, L. *Carbon* **2002**, *40*, 1697−1714.
(18) Souza, A. G.; Jorio, A.; Swan, A. K.; Unlu, M. S.; Goldberg, B. B.; Saito, R.; Hafner, J. H.; Lieber, C. M.; Pimenta, M. A.; Dresselhaus, G.; Dresselhaus, M. S. *Phys. Rev. B* **2002**, *65*, art. no.-085417.
(19) Saito, R.; Grueneis, A.; Cancado, L. G.; Pimenta, M. A.; Jorio, A.; Dresselhaus, G.; Dresselhaus, M. S.; Souza, A. G. *Mol. Cryst. Liq. Cryst.* **2002**, *387*, 287−296.
(20) Kuzmany, H.; Plank, W.; Hulman, M.; Kramberger, C.; Gruneis, A.; Pichler, T.; Peterlik, H.; Kataura, H.; Achiba, Y. *Eur. Phys. J. B* **2001**, *22*, 307−320.
(21) Dresselhaus, M. S.; Jorio, A.; Dresselhaus, G.; Saito, R.; Souza, A.; Pimenta, M. A. *Mol. Cryst. Liq. Cryst.* **2002**, *387*, 245−253.
(22) Dresselhaus, M. S.; Dresselhaus, G.; Jorio, A.; Souza, A. G.; Saito, R. *Carbon* **2002**, *40*, 2043−2061.
(23) Brown, S. D. M.; Jorio, A.; Corio, P.; Dresselhaus, M. S.; Dresselhaus, G.; Saito, R.; Kneipp, K. *Phys. Rev. B* **2001**, *63*.
(24) McCreery, R. L. Photometric Standards for Raman Spectroscopy. In *Handbook of Vibrational Spectroscopy*; Chalmers, J. M., Griffiths, P. R., Eds.; Wiley & Sons: Chichester, England, 2002.
(25) Bronikowski, M. J.; Willis, P. A.; Colbert, D. T.; Smith, K. A.; Smalley, R. E. *J. Vac. Sci. Technol.* **2001**, *19*, 1800−1805.
(26) Strano, M. S.; Huffman, C. B.; Moore, V. C.; O'Connell, M. J.; Haroz, E. H.; Hubbard, J.; Miller, M.; Rialon, K.; Kittrell, C.; Ramesh, S.; Hauge, R. H.; Smalley, R. E. *J. Phys. Chem. B* **2003**, *107*, 6979−6985.
(27) Fraction f36 has a peak at 1061 nm that was unassigned previously (marked by *). The lack of relative shifting between emission features causes us to reject the possibility that this feature is less shifted (10, 2). It is possible that this feature is the (11, 0) nanotube at a nominal v1(c1) transition when unshifted to a lower energy of 1039 nm and a v2(c2) transition at 741 nm. The origin of this feature can be identified using fluorescence excitation profiles, and this work is currently underway.
(28) Jorio, A.; Souza, A. G.; Dresselhaus, G.; Dresselhaus, M. S.; Swan, A. K.; Unlu, M. S.; Goldberg, B. B.; Pimenta, M. A.; Hafner, J. H.; Lieber, C. M.; Saito, R. *Phys. Rev. B* **2002**, *65*, p. art. no.-155412.
(29) Reich, S.; Thomsen, C.; Ordejon, P. *Phys. Rev. B* **2001**, *6419*, p. art. no.-195416.

(30) Dresselhaus, M. S.; Dresselhaus, G.; Jorio, A.; Souza Filho, A. G.; Pimenta, M. A.; Saito, R. *Acc. Chem. Res.* **2002**, *35*, 1070−1078.
(31) Souza, A. G.; Jorio, A.; Dressselhaus, G.; Dresselhaus, M. S.; Saito, R.; Swan, A. K.; Unlu, M. S.; Goldberg, B. B.; Hafner, J. H.; Lieber, C. M.; Pimenta, M. A. *Phys. Rev. B* **2002**, *6503*, p. art. no.-035404.
(32) Cowley, J. M.; Nikolaev, P.; Thess, A.; Smalley, R. E. *Chem. Phys. Lett.* **1997**, *265*, 379−384.
(33) We note that in normalizing these fractions to their solvent D−O Raman mode that f39 is considerably more concentrated than the starting material. This may be an artifact of the reconcentration process that attempted to equalize the total added volume but apparently created disparities in the concentrations of the SWNT material (see refs 6 and 7). Nontube impurities, particularly fullerene fragments, may elute from the column first and change the mass concentration of the early fractions. All of the above analysis in this work considers relative peak intensities or shifts and is therefore unaffected by this disparity with this one fraction.
(34) Jorio, A.; Matinaga, F. M.; Righi, A.; Dantas, M. S. S.; Pimenta, M. A.; Souza Filho, A. G.; Mendes Filho, J.; Hefner, J. H.; Lieber, C. M.; Saito, R.; Dresselhaus, G.; Dresselhaus, M. S. *Braz. J. Phys.* **2002**, *32*, 921−924.

NL034937K